Journal of Catalysis 260 (2008) 236–244

Contents lists available at ScienceDirect

Journal of Catalysis

www.elsevier.com/locate/jcat

Mechanochemical activation of MoS_2—Surface properties and catalytic activities in hydrogenation and isomerization of alkenes and in H_2/D_2 exchange

Mykola Polyakov [a], Sylvio Indris [b,1], Stefanie Schwamborn [a], Aliaksei Mazheika [a,2], Martha Poisot [c,3], Lorenz Kienle [d], Wolfgang Bensch [c], Martin Muhler [a], Wolfgang Grünert [a,*]

[a] Laboratory of Industrial Chemistry, Ruhr University Bochum, P.O. Box 102148, D-44780 Bochum, Germany
[b] Institute of Physical Chemistry and Electrochemistry, Leibniz University Hannover, Hannover, Germany
[c] Institute of Inorganic Chemistry, Christian Albrechts University Kiel, Kiel, Germany
[d] Institute of Materials Science, Christian Albrechts University Kiel, Kiel, Germany

ARTICLE INFO

Article history:
Received 4 June 2008
Revised 9 September 2008
Accepted 7 October 2008
Available online 23 October 2008

Keywords:
Molybdenum sulfide
Active sites
Ball milling
TEM
Hydrogenation
H_2/D_2 scrambling
Double-bond isomerization

ABSTRACT

High-energy ball milling has been employed to convert a microcrystalline, stoichiometric (S/Mo = 2), catalytically completely inactive MoS_2 (prepared by high-temperature decomposition of ammonium tetrathiomolybdate, ATM) into an active catalyst, the activity profile of which was studied with test reactions (ethylene hydrogenation, H_2/D_2 scrambling, *cis–trans* isomerization of *cis*-but-2-ene, double-bond isomerization of 2-methyl-1-butene). Structural and surface properties of the materials were studied by XRD, SEM, TEM, XPS, nitrogen physisorption, oxygen chemisorption, and isotope exchange with D_2 (quantity of exchangeable surface hydrogen). The reaction rates obtained after mechanochemical activation were compared with data from a reference MoS_2 made by low-temperature decomposition of ATM. Ball-milled MoS_2 became active for most of the test reactions (except double-bond isomerization) only after reductive treatments that were effective also with the reference MoS_2. After identical treatments, the ball-milled MoS_2 was much more active in hydrogenation than the reference MoS_2, whereas H_2/D_2 scrambling proceeded more slowly, and *cis–trans* isomerization not at all. On the basis of earlier conclusions about the site selectivity of these reactions, the activity pattern indicates that mechanochemical activation led to a site structure dominated by sites with multiple vacancies whereas single-vacancy sites were not present at all, which is in agreement with TEM results showing highly defective bent nanoslab structures after ball milling. The results confirm that ethylene hydrogenation, H_2/D_2 scrambling and *cis–trans* isomerization of *cis*-but-2-ene may be employed as test reactions for sites on MoS_2 surfaces whereas data for the double-bond shift in 2-methyl-1-butene suggest that the Brønsted sites catalyzing this reaction are related to structural defects rather than to the regular MoS_2 structure.

1. Introduction

The catalytic activity of solid catalysts is supported by sites which are often conceived to be surface defects. Highly exposed metal atoms are known to exhibit extraordinary, sometimes undesired activities in metal-catalyzed reactions. Vacancies in the external anion layer are the prerequisite for oxide and sulfide catalysts to show their activities in many reactions. Such coordinatively unsaturated sites are either produced by thermal pretreatments (hydrogenation, evacuation) or they form under the influence of the reaction medium, which will produce a defect structure close to the equilibrium structure under the prevailing conditions.

Mechanochemical activation is an interesting alternative to thermal routes of active site formation. The defect structure produced by the treatment (e.g., milling) typically at low temperature is far from the equilibrium situation. For reactions proceeding under conditions too mild to induce mobility in the surface layer, catalytic activities and activity patterns in complex reactions may be expected to deviate strongly from those seen on thermally activated catalyst surfaces. Unusual activities may be obtained even under conditions sufficient to bring surface defect distributions to equilibrium because these may deviate from distributions on the surfaces of perfect solids due to bulk structural defects left behind by the mechanical treatment.

The use of high-energy milling in catalyst preparation and activation has a long tradition [1], e.g. for synthesis of mixed

* Corresponding author. Fax: +49 234 321 4115.
E-mail address: w.gruenert@techem.rub.de (W. Grünert).
[1] Present address: Forschungszentrum Karlsruhe, Institut für Nanotechnologie, P.O. Box 3640, 76021 Karlsruhe, Germany.
[2] Present address: Research Institute for Physical Chemical Problems of the Belarusian State University, 14 Leningradskaya Street, 220050 Minsk, Belarus.
[3] Present address: Universidad del Papaloapan, Circuito Central 200, Parque Industrial Tuxtepec 68301, Oaxaca, Mexico.

0021-9517/$ – see front matter
doi:10.1016/j.jcat.2008.10.005

phases (perovskites [2], Ce–Zr mixed oxides [3], hydrogen storage materials [4]), for the preparation of Ziegler–Natta polymerization catalysts [5], and for the activation of known catalytic phases, e.g. vanadium phosphates for selective oxidation [6], perovskites for catalytic combustion [7], SiO_2-supported MoO_x for selective methane oxidation [8], or TiO_2 for photocatalytic hydrocarbon combustion [9]. Mechanochemical stages have been considered even for the preparation of catalysts for ammonia [10] and methanol synthesis [11].

Less work has been done with sulfide materials. Kuriki et al. activated crystalline MoS_2 in different mills and characterized the products by XRD, TEM and a sedimentation technique (for particle size distribution) [12]. They found the activity in 1-methylnaphthalene hydrogenation drastically increased. According to Kouzo et al., the activity (on an equivalent weight of Mo basis) of mechanochemically activated MoS_2 in dibenzothiophene dehydrodesulfurization exceeded that of Al_2O_3-supported MoS_2 and competed even with an industrial Co–Mo/Al_2O_3 catalyst [13]. A strong preference of the hydrogenative pathway over the direct desulfurization route in the milled MoS_2 indicated differences in the site distribution between supported and mechanically activated MoS_2. In the present paper, a completely inactive microcrystalline MoS_2 was activated by high-energy ball milling and characterized by different methods, including TEM. Its catalytic activities in test reactions known to proceed on different sites (ethylene hydrogenation, *cis–trans* isomerization of *cis*-but-2-ene, H_2/D_2 isotope exchange [14–16], and double-bond isomerization of 2-methyl-1-butene) were compared with those found over a nano-crystalline MoS_2 from a low-temperature preparation. It will be shown that the mechanochemical treatment creates a site structure favoring highly exposed Mo sites at the expense of sites with a low number of vacancies.

2. Experimental

2.1. Materials

The initial MoS_2 was prepared by a high-temperature decomposition of ammonium tetrathiomolybdate ($(NH_4)_2MoS_4$, ATM). The precursor was heated in flowing Ar to 723 K in 15 h, after 24 h at this temperature further to 1273 K in 22 h, and slowly cooled down after 60 h at 1273 K (total duration of synthesis—7 days). 1.5 g of this MoS_2 were milled in a high-energy ball mill with a corundum vial and ball (Spex 8000, ball-to-powder weight ratio—3:1). The milling was performed for 8 h in Ar atmosphere without additives. The mechanically activated MoS_2 ("m-MoS_2") was further handled in Ar and stored in a glove box to avoid oxidation of its surface. A sample of m-MoS_2 was suspended in ethanol and treated in an ultrasonic bath (Sonorex RK 103H of Bandelin Co., Germany) at 35 kHz and 100 W for 1 h to break supposed particle aggregations ("m-MoS_2(us)").

The data will be compared with results obtained with a MoS_2 material prepared via low-temperature decomposition of $(NH_4)_2MoS_4$ in inert gas as described earlier in the literature [17]. Detailed information on the preparation of this low-temperature (LT-)MoS_2 (maximum temperature involved—773 K), its surface properties and catalytic behavior have been published earlier [14,18]. The data cited in the present paper were almost exclusively measured with a batch labeled $MoS_2(A_1)$ in [14,18], only in one case (Fig. 8a), additional results from another batch prepared under a slightly different temperature regime (MoS_2(B) in [14,18], labeled LT-MoS_2* here) will be given.

2.2. Methods

Chemical elemental analyses were made with a EURO Vector EA Combustion analyzer using 2–3 mg of sample, which were heated up to 1273 K under oxygen atmosphere. The gases emitted (SO_2, CO/CO_2, H_2O, NO/NO_2) were separated gas-chromatographically and detected with a thermo-conductivity cell. *X-ray powder patterns* were recorded with a Phillips X'Pert diffractometer (MoS_2, m-MoS_2) or with a STOE STADI-P instrument (LT-MoS_2) using monochromatized Cu$K_{\alpha 1}$ radiation ($\lambda = 1.54056$ Å). *Scanning electron microscopy* images were obtained with a Phillips ESEM XL30 Scanning electron microscope.

Transmission electron microscopy studies were performed with a Philips CM 30ST microscope (LaB_6 cathode, 300 kV, C_S = 1.15 mm), to which the samples were inserted on copper/holy carbon grids. SAED (selected area electron diffraction) and PED (precession electron diffraction [19–21]) were carried out using a diaphragm which limited the diffraction to a circular area of 2500 Å in diameter. HRTEM micrographs were evaluated (including Fourier filtering) with the programs Digital Micrograph 3.6.1 (Gatan) or Crisp (Calidris).

N_2 physisorption isotherms were measured with a Quantachrome Autosorb-1 MB instrument. Prior to the measurements, the samples were evacuated at 523 K if not stated otherwise. Pore size distributions were derived from the desorption branches using the BJH formalism [22]. For the initial MoS_2, the BET surface area was determined by Kr physisorption. *X-ray photoelectron spectra* (Mo 3d, S 2p, O 1s, N 1s, and C 1s lines) were recorded with a Scienta/Specs/Prevac Surface analysis system using monochromatized Al radiation. Samples were transferred from the glove box to the load lock of the instrument by means of a sample transfer shuttle (Prevac, with in-house modifications), cf. [18].

Catalytic and related data were measured in a setup characterized by facile switching options between batch (cycle) and flow regimes and between thermoevacuation treatment and reaction (for more details see [14]). The setup allowed to perform pulse oxygen chemisorption (OCS) prior to catalysis (reactivation after OCS by reduction in 10% H_2/He at 473 K for 1 h) and to load or withdraw air-sensitive samples from (or to) a glove box. MoS_2 (typically 0.1 g) was investigated after three different activation treatments: (a) evacuation (rotary pump) at 723 K for 4 h ("$\mathbf{V}_{723}$"), (b) thermoevacuation with subsequent reduction in H_2 (10% in He) at 573 K for 3 h ("$\mathbf{V}_{723}/\mathbf{R}_{573}$"), and (c) reduction in H_2 (10% in He) for 3 h at 573 K *without* previous thermoevacuation ("$\mathbf{R}_{573}$"). After the activation, one or more of the following procedures were performed:

- *Oxygen chemisorption (OCS)* in pulse mode at 273 K, with mass-spectrometric detection (Pfeiffer QME 125).
- *Determination of exchangeable surface hydrogen (H-Exc)*; the catalysts were cooled to 473 K in 10% H_2/Ar where the carrier gas was replaced by pure Ar keeping the temperature until the $m/e = 2$ QMS signal was constant. After cooling to room temperature, the reactor was reheated up to 573 K in a slow flow of D_2 (10% in Ar), and the quantity of HD evolved was determined by calibrated mass spectrometry.
- *Catalysis*. All reactions were studied in recycle mode. The procedure has been described in detail in [14]. Briefly, the reaction cycle was filled with the required reaction mixture while the catalyst was heated to the desired temperature in a separate reactor loop under helium. The kinetic run was started by switching the reactor loop into the cycle, which caused mixing perturbations only in the first minute. In Table 1, the reactions studied are listed together with the initial reactant concentrations resulting after mixing of reaction cycle and catalyst loop contents. It should be noted that all test reactions were performed after activations at temperatures above the reaction temperature, therefore, changes of the site structure during reaction were not expected. Moreover, except for H_2/D_2 scrambling the test reactions suffered deactivation by hydrocarbon

Table 1
Test reactions and parameters of their experimental realization.

Reaction	Initial concentrations (vol% in He)	Product analysis
Ethylene hydrogenation	Ethylene—2.4, H_2—8	QMS[a]
H_2/D_2 scrambling	H_2—4, D_2—4	QMS[a]
Cis–trans isomerization of *cis*-but-2-ene	*Cis*-butene—0.004, H_2—8	GC[b]
Double-bond isomerization of 2-methyl-1-butene[c]	2-methyl-1-butene—≈0.1	GC[b]

[a] Calibrated mass spectrometry.
[b] 30 m 0.5 mm GSQ capillary column, 400–410 K.
[c] To 2-methyl-2-butene.

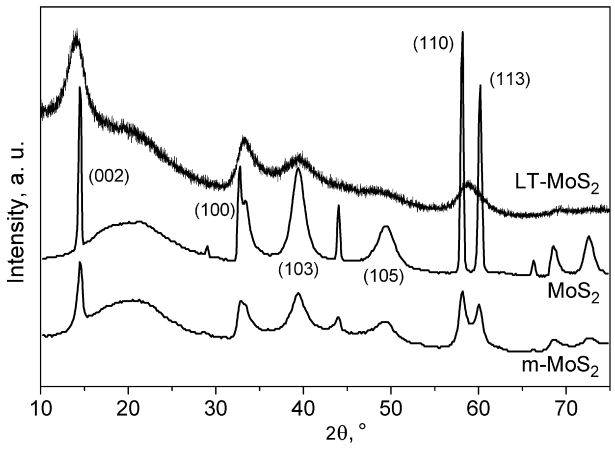

Fig. 1. X-ray diffractograms of MoS_2 prepared via different routes.

deposition to a certain extent (cf. also [14], and below), hence, only initial reaction rates could be used to characterize the surface.

Except for the 2-methyl-1-butene isomerization, kinetic data for conversions up to 20% were used to evaluate first-order rate constants [14], including H_2/D_2 scrambling where a first-order kinetics has been reported earlier in the literature [23]. 2-Methyl-1-butene isomerization on mechanochemically activated MoS_2 was extremely rapid, with equilibrium conversions of nearly 90% achieved already after 4 min in some cases, and exhibited strong deactivation which prevented measuring precise reaction rates even in flow mode. The data given below for this reaction have therefore to be classified as estimates rather than as accurate data. Nevertheless, due to the large differences between the materials studied, some relevant conclusions could be drawn.

3. Results and discussion

3.1. Physicochemical characterization

Elemental analysis showed that mechanical milling caused a considerable sulfur loss in the MoS_2 material. While the initial MoS_2 had a S/Mo ratio of 2.01, this quantity fell to 1.8 after the mechanochemical activation. For as-synthesized LT-MoS_2, a Mo/S ratio of 2.40 was determined, which fell to 2.04…2.11 after the thermal activations employed here [18].

The *X-ray diffractograms* of the different MoS_2 samples are compared in Fig. 1. The effect of milling on the crystalline MoS_2 is quite obvious: all initially narrow reflections are lowered and broadened. The effect of the mechanical treatments on the coherence lengths is, however, moderate and LT-MoS_2 gives signals with much larger peak widths. The coherence lengths estimated for the (002) reflection (stacking direction) via the Scherrer equation are ≈28 nm before and ≈17 nm after milling, whereas the data of LT-MoS_2 result in a primary particle size in the order of 3 nm. The moderate effects of the mechanochemical treatment may be explained by the observation that the coherence length was far below the crystallite size already in the initial MoS_2 (30 nm *vs.* 30 μm), i.e. stacking faults were abundant already in the seemingly perfect crystals (*vide infra*).

In Fig. 2, *scanning electron micrographs* of the crystalline MoS_2 in the initial state (a) and after milling (b) are compared with images of LT-MoS_2. The initial MoS_2 consists of nice hexagonal platelets, the diameter of which varies in a broad range from 10 to 50 μm. After milling, no more regular shapes are left, and irregular chunks of matter are mixed with chips of μm size. The LT-MoS_2 consists of flat bars evocating of wooden boards (c), with a rough and porous surface.

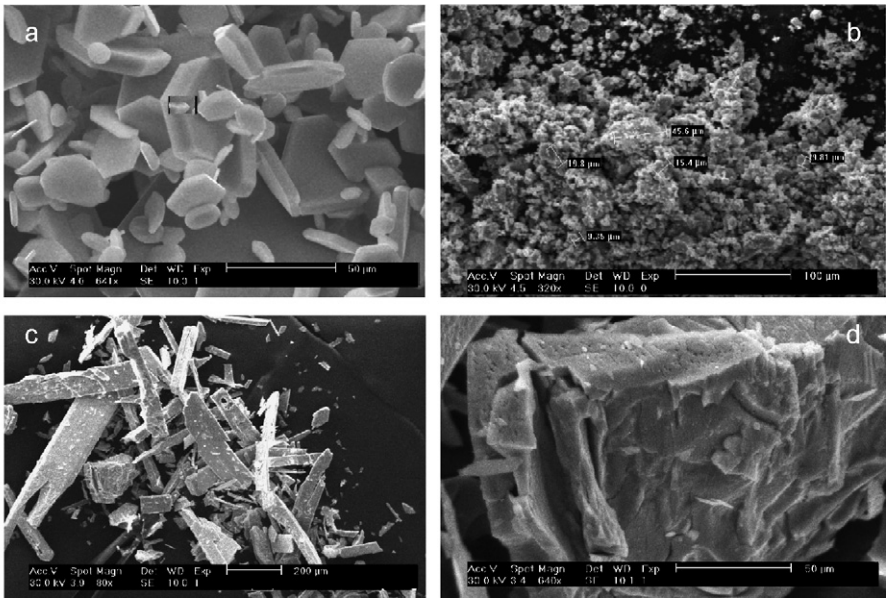

Fig. 2. Scanning electron micrographs of MoS_2 materials employed: (a) (microcrystalline) MoS_2, (b) m-MoS_2 made by high-energy ball milling of MoS_2 (cf. a), (c) and (d) LT-MoS_2, made by low-temperature decomposition of ATM, in different magnifications.

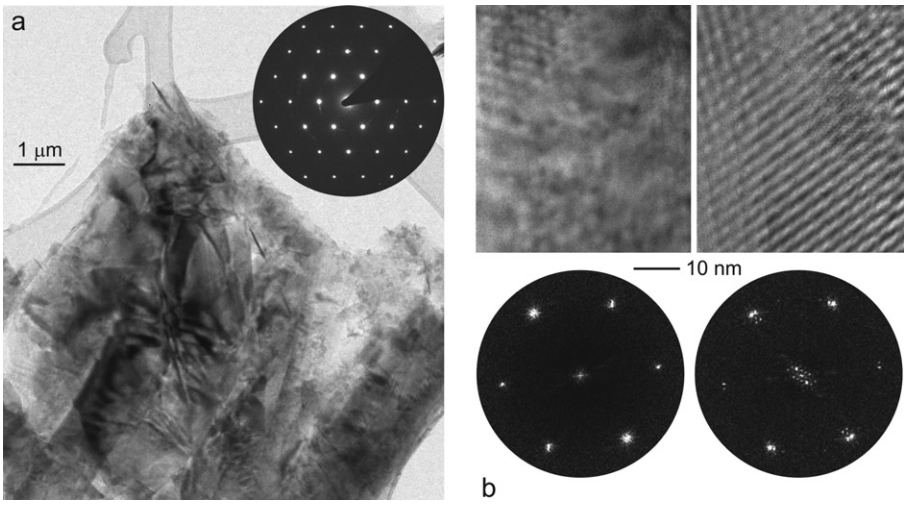

Fig. 3. TEM micrographs of microcrystalline MoS_2: (a) bright-field survey image of a typical microcrystal in [001] zone axis orientation, insert—PED pattern, (b) high-resolution micrographs and Fourier transforms recorded on different areas of the same microcrystal, left—weak misfit, right—strong misfit.

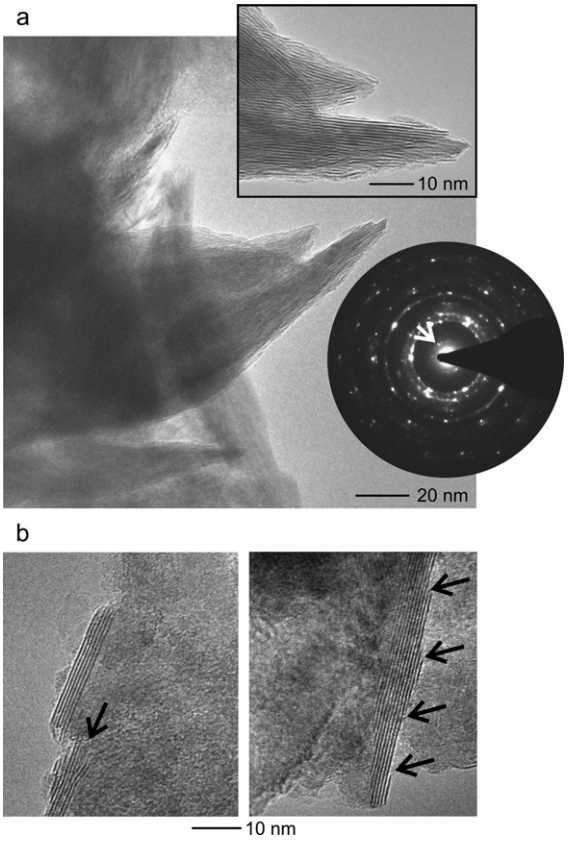

Fig. 4. TEM micrographs of m-MoS_2: (a) high resolution micrograph (with enlarged cutout) and SAED pattern recorded on nanoslabs, (b) characteristic crystal defects of nanoslabs.

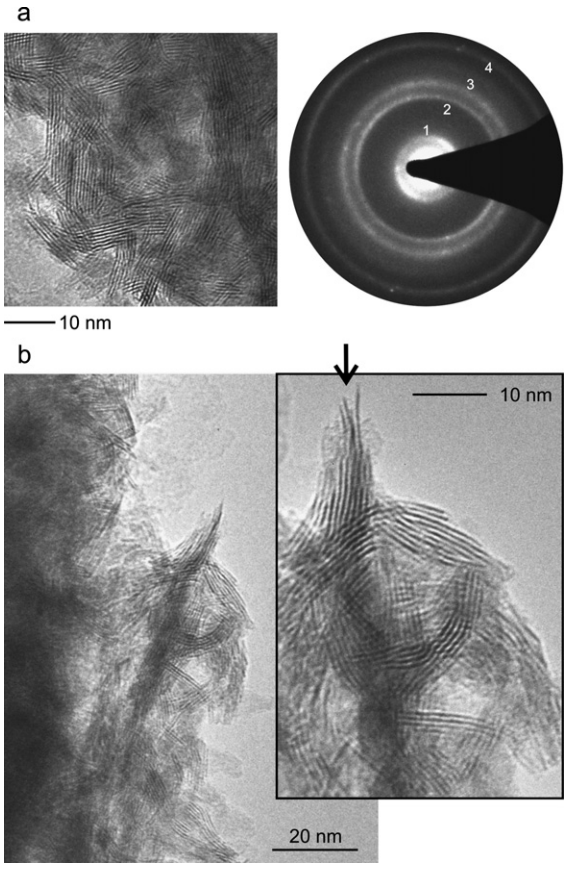

Fig. 5. TEM micrographs of LT-MoS_2: (a) SAED pattern and high resolution micrograph recorded on an aggregation of nanoslabs, (b) split nanoslab projecting from an aggregation of bent nanoslabs.

TEM micrographs of the MoS_2 materials studied are presented in Figs. 3–5. Thin platelets with square dimensions of several microns and (001) top and bottom surfaces were the predominant morphology observed in the microcrystalline MoS_2 (Fig. 3a), nanoslabs in their preferred [*uv*0] zone axis orientation were never seen. Diffraction patterns, when taken on selected areas with uniform bright field contrast, correlated well with MoS_2–2H (cf. insert). Variations of the bright-field contrast based on the misfit of rotated (001) layers and other planar defects occurred frequently (stripes in Fig. 3a). In such cases, Moiré contrast was clearly seen in the high resolution mode, and diffraction patterns and Fourier transforms exhibited satellites next to the main structure reflections. These phenomena varied locally inside the same crystallite as depicted in Fig. 3b for areas with weak (left) and strong (right) misfit. This explains the above-mentioned strong divergence between crystallite size and coherence lengths observed by XRD.

In m-MoS_2 a majority of aggregated MoS_2 nanoslabs was found together with extended platelets apparently left over from the initial material. The rotational disorder of the nanoslabs produced

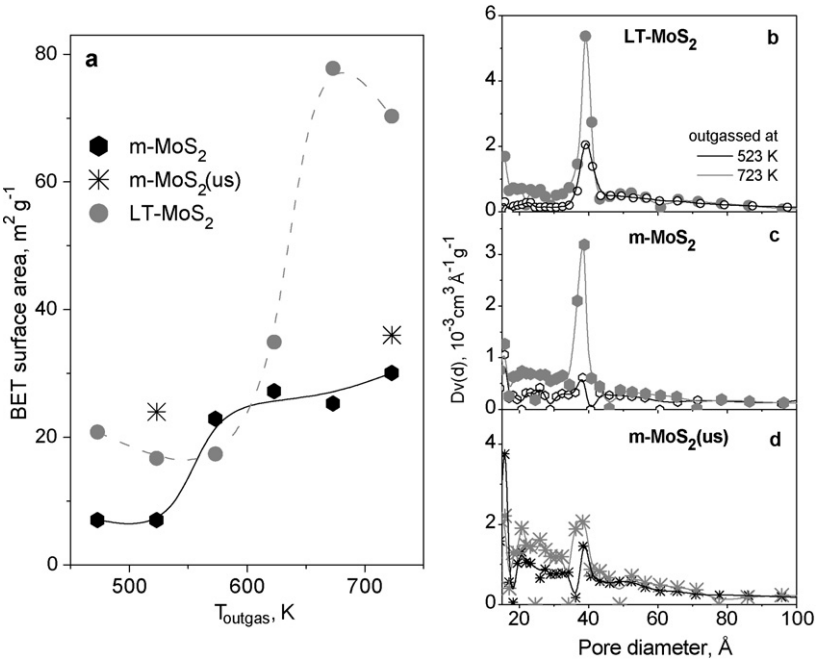

Fig. 6. Porosity analysis of MoS_2 activated by high-energy ball milling, compared with MoS_2 prepared by low-temperature decomposition of ATM (LT-MoS_2): (a) development of BET surface area with temperature of thermoevacuation for two batches; (b, c, d) pore-size distributions (BJH, desorption branch) of: LT-MoS_2 (b), m-MoS_2 (c), and m-MoS_2 after ultrasonic treatment (c) after evacuation at different temperatures.

diffuse intensity on concentric circles in the diffraction patterns (cf. insert to Fig. 4a), which was superimposed by the Bragg reflections of the platelets. Note that due to the orientation of the nanoslabs along zone axes [*uv*0] intensity for reflections 002 (d(002)exp. = 6.17 Å, calculated [24]—6.15 Å) was significantly excited, see arrow in Fig. 4a. HRTEM micrographs (see enlarged cutout in Fig. 4a, and Fig. 4b) imaged the consecutive (001) layers as parallel lines with a distance of 6.15 Å. As a rule, the nanoslabs were strongly bent and contained dislocations. Additionally, splitting of the nanoslabs and a stepwise truncations of the (001) layers occurred at the surface, see arrows in Fig. 4b. Such characteristic surface structure produced sharp edges as also seen at the tips of the nanoslabs, cf. Fig. 4a.

Morphology and real structure of the MoS_2 species in sample LT-MoS_2 were strongly related to the nanoslabs observed in m-MoS_2, however, extended crystals were rarely observed. Therefore, the SAED patterns recorded on aggregates exclusively showed diffuse rings (Fig. 5a) with diameters correlating well with MoS_2. The high resolution micrographs of Fig. 5 depict aggregates of nanoslabs built from 3–7 (001) layers and with average aspect ratios up to 10. Again, bending and splitting of the nanoslabs was frequently observed, cf. arrow in enlarged cutout of Fig. 5b. These structural defects well account for the small coherence lengths found for LT-MoS_2 by XRD whereas the XRD line shapes of m-MoS_2 may be understood as a superposition of narrow and broad contributions (residual platelets and nanoslabs, respectively).

The *BET surface area* of MoS_2 was as low as 0.3 $m^2 g^{-1}$ and did not change significantly upon thermoevacuation at 723 K. After milling, the BET surface area was considerably larger (7 $m^2 g^{-1}$), but this value is far below data reported by previous authors after wet milling (98 $m^2 g^{-1}$ [13], 120 $m^2 g^{-1}$ [12]). Ultrasonic treatment of m-MoS_2 increased its BET surface area to 24 $m^2 g^{-1}$ (Fig. 6a).

It has been reported in [18] that outgassing of LT-MoS_2 at higher temperatures causes a pronounced enhancement of the BET surface area by formation of new mesopores, in particular of sizes around 4 nm. The corresponding data have been included in Figs. 6a and 6b. The milled m-MoS_2 showed a similar behavior (Fig. 6c) although this sample originated from a material that was completely stable under vacuum at 723 K. After ultrasonic treatment in ethanol, the resulting m-MoS_2(us) exhibited completely different properties (Fig. 6d). The enhancement of the BET surface area by the ultrasonic treatment was due to contributions from a wide range of pore sizes including apparently micropores (where the BJH formalism gives erroneous results). This unspecific effect may at least partly have been caused also by variations in the intra-particle voids, which can contribute to the capillary phenomena. No preferred pore width was generated by the ultrasonic treatment, and further thermoevacuation created such pore system only to a minor extent. This suggests that the reactivity of the material was significantly changed by the treatment.

XP spectra of MoS_2 have been recorded in the initial state and after milling to check for possible contaminations by the milling process. The spectrum of the initial MoS_2 was shown in [18] (cf. Fig. 3 there, label "MoS_2(cryst)"). It exhibited only signals attributable to the sulfide. Small satellites, which were observed at the low binding-energy side of all lines, may arise from a differential charging effect, but do not indicate contaminations. After milling, no impurity elements were found, and the satellites mentioned had disappeared (spectra not shown). In the S 2p region, the sulfide signal was accompanied by a weak signal at a binding energy typical of sulfate. This shows that surface oxidation could not be completely avoided, which is not unexpected for a highly defective surface. It has been shown in [18] that reduction in hydrogen at 573 K effectively removes surface sulfate species, therefore the surface was clean in all experiments that involved such activation.

Oxygen chemisorption capacities and concentrations of *exchangeable hydrogen* after the activation treatments are presented in Table 2. The initial MoS_2 did not adsorb oxygen after any of the thermal activations applied, and exchangeable hydrogen was not observed. After the mechanochemical treatment, sites for oxygen chemisorption were created only by the standard activations. OCS capacities and amounts of exchangeable hydrogen were lower than on LT-MoS_2. Whereas the data for exchangeable hydrogen seem to be related between m-MoS_2 and LT-MoS_2, the former rendering 35–45% of the latter, there was no such relation in their OCS capacities (65% after $\mathbf{V}_{723}/\mathbf{R}_{573}$, 30% after $\mathbf{R}_{573}$). Taking into account

Table 2
Oxygen chemisorption capacity (OCS) and concentration of exchangeable hydrogen (H-exc) after different activation treatments.

Activation, sample	Surface area ($m^2\,g^{-1}$)	OCS ($\mu mol\,g^{-1}$)	H-exc ($\mu mol\,g^{-1}$)
$\mathbf{V}_{723}/\mathbf{R}_{573}$			
MoS_2	≈0.3[a]	0	0
m-MoS_2	30[a]	18	40
LT-MoS_2	70[a,b]	28	115
$\mathbf{R}_{573}$			
MoS_2	n.d.	0	0
m-MoS_2	n.d.	17	48
LT-MoS_2	21[b]	60	109

[a] After $\mathbf{V}_{723}$.
[b] From [18].

that after $\mathbf{V}_{723}/\mathbf{R}_{573}$ the BET surface area of m-MoS_2 was ca. 40% that of LT-MoS_2 (Fig. 6, data after evacuation at 723 K, cf. Table 2), one may conclude that after this activation the density of vacancies was larger on m-MoS_2 while that of exchangeable hydrogen was similar on both samples. It should be kept in mind, however, that opposed to the OCS capacity the amount of exchangeable hydrogen exhibited extreme variations between different LT-MoS_2 batches [18], hence, any conclusion related to this quantity should be drawn with caution.

After the ultrasonic treatment of m-MoS_2, oxygen chemisorption was not observed either after $\mathbf{V}_{723}/\mathbf{R}_{573}$, or after $\mathbf{R}_{573}$. Probably, the ethanol in which the sample was suspended underwent strong interactions with the surface which prevented the exposition of Mo ions by the treatments employed. As a consequence, the ultrasonic treatment suppressed any catalytic activity as well.

3.2. Catalysis

In the following, the catalytic behavior of mechanochemically activated microcrystalline MoS_2 is compared with that of LT-MoS_2. For reactions catalyzed by coordinatively unsaturated ions (Mo_{cus}), which are poisoned by oxygen, more information about the catalytic properties of LT-MoS_2 is given in [14]. Our data on the isomerization of 2-methyl-1-butene, which is an acid-catalyzed reaction and not poisoned by oxygen [15,16] are published here first for both catalysts.

The initial microcrystalline MoS_2 was inactive in all reactions *including* the acid-catalyzed 2-methyl-1-butene isomerization. The same is true for the ball-milled MoS_2 after ultrasonic treatment as mentioned above.

3.2.1. Ethylene hydrogenation

The mechanochemical treatment resulted in a catalyst that outperformed LT-MoS_2 in ethylene hydrogenation after identical thermal activations. The activation energies found for both catalysts, however, were identical in the limits of experimental error (Fig. 7a, Table 3), which suggests that only one type of active site is responsible for the hydrogenation on all surfaces, and the different activities might be discussed in terms of site abundance. m-MoS_2 activated by $\mathbf{V}_{723}/\mathbf{R}_{573}$ could well compete even with the most active states found with the low-temperature preparation: As shown in [14], reversal of thermoevacuation and reduction of LT-MoS_2 (i.e., $\mathbf{R}_{573}/\mathbf{V}_{723}$) led to a catalyst surface with an almost 25 fold higher hydrogenation activity, but low activity in *cis–trans* isomerization of *cis*-but-2-ene (see also footnote b in Table 3). The rate constant of m-MoS_2 after $\mathbf{V}_{723}/\mathbf{R}_{573}$ ($3\times10^{-2}\ l\,g^{-1}\,s^{-1}$, at 473 K) was of the same order of magnitude as the highest seen with LT-MoS_2 (after $\mathbf{R}_{573}/\mathbf{V}_{723}$, $7.7\times10^{-2}\ l\,g^{-1}\,s^{-1}$), and due to the smaller OCS capacity of the former (cf. Table 1), the "rate per vacancy" r_0/OCS obtained with m-MoS_2 after $\mathbf{V}_{723}/\mathbf{R}_{573}$ was about 2/3 of the highest ever seen with LT-MoS_2 (see footnote b in Table 3).

Extensive studies on adsorption and reactivity of LT-MoS_2 in the test reactions used here have led us to propose that ethylene hydrogenation can be used as a test reaction for Mo_{cus} with three vacancies (^{3}M sites). Analogously, *cis–trans* isomerization activity is indicative of ^{1}M sites while H_2/D_2 scrambling may proceed both on ^{2}M and ^{3}M sites [14,18]. Given the invariability of the activation energies in ethylene hydrogenation (Fig. 7a, Table 3), the increased hydrogenation activity after identical activations suggests a shift towards higher exposed sites in the Mo_{cus} distribution of m-MoS_2 as compared with LT-MoS_2. This is what should be expected from the S/Mo ratios, which remained ⩾2.0 after all activations performed with LT-MoS_2 while that of m-MoS_2 was 1.8 already before any thermal treatment. It should be noted that m-MoS_2 achieved reaction rates per vacancy that are comparable but still smaller than the highest seen with LT-MoS_2. This gives rise to the speculation that the surface of m-MoS_2 after $\mathbf{V}_{723}/\mathbf{R}_{573}$ might contain higher exposed Mo sites (^{4}M), which might be inactive for hydro-

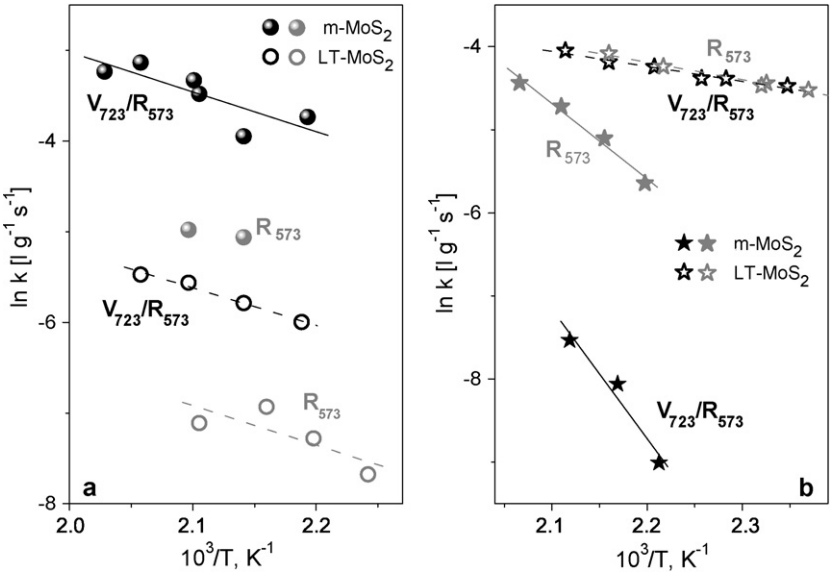

Fig. 7. Relation between activation procedure and catalytic activity for ball-milled MoS_2(m-MoS_2) and LT-MoS_2, made by low-temperature decomposition of ATM: (a) ethylene hydrogenation; (b) H_2/D_2 scrambling.

Table 3
Catalytic activity of m-MoS_2 and LT-MoS_2: comparison of kinetic data.

Reaction	Quantity	LT-MoS_2		m-MoS_2	
		$\mathbf{R}_{573}$	$\mathbf{V}_{723}/\mathbf{R}_{573}$	$\mathbf{R}_{573}$	$\mathbf{V}_{723}/\mathbf{R}_{573}$
Ethylene hydrogenation	10^3k ($l\,g^{-1}\,s^{-1}$) at 473 K[a]	0.94	3.4[b]	6.7	30
	10^2r_0/OCS (s^{-1}) at 473 K[a]	1.5	12[b]	38	160
	E_A ($kJ\,mol^{-1}$)	36	34	n.d.	36
H_2/D_2 scrambling	10^3k ($l\,g^{-1}\,s^{-1}$) at 473 K[a]	18[c]	19[c]	8.4[c]	0.64
	r_0/OCS (s^{-1}) at 473 K[a]	0.5_5[c]	1.2_5[c]	1.8[c]	0.13
	E_A ($kJ\,mol^{-1}$)	17.5[c]	15[c]	75[c]	(130)
2-Butene isomerization	10^3k ($l\,g^{-1}\,s^{-1}$) at 473 K[a]	4.1	1.3	0	0
	10^4r_0/OCS (s^{-1}) at 473 K[a]	1.1	0.75	0	0
	E_A ($kJ\,mol^{-1}$)	51	54	–	–
2-Methyl-1-butene isomerization	10^3k ($l\,g^{-1}\,s^{-1}$) at 473 K[a]	0.52	1.75	11	
	E_A ($kJ\,mol^{-1}$)	49	57	48	

[a] Interpolated from Arrhenius curve.
[b] Highest ethylene hydrogenation activity achieved by reversal of treatments ($\mathbf{R}_{573}/\mathbf{V}_{723}$)—$10^3k$ (473 K) = 77 $l\,g^{-1}\,s^{-1}$, 10^2r_0/OCS = 254 s^{-1}.
[c] Influenced by mass transport limitations, see text.

genation. The inactivity of ^{4}M sites has earlier been proposed by Jalowiecki et al. [25].

3.2.2. *cis–trans* isomerization of cis-but-2-ene

The conclusion that the activations used produce predominantly highly exposed Mo_{cus} on the surface of m-MoS_2 is further substantiated by the observations made with *cis–trans* isomerization. LT-MoS_2 was best activated for this reaction by mild reduction, e.g., mere thermoevacuation ($\mathbf{V}_{723}$), whereas an additional subsequent reduction in hydrogen at 573 K caused the isomerization activity to decrease [14]. m-MoS_2 could not be activated at all for this reaction neither by $\mathbf{R}_{573}$ nor by $\mathbf{V}_{723}/\mathbf{R}_{573}$, no conversion was seen at 473 K in runs of more than 90 min duration. Apparently, no ^{1}M sites were formed on its surface. This might have been expected given the low S/Mo ratio of m-MoS_2 already before thermal activation (1.8), but it has yet to be elucidated if it is due to the non-equilibrium character of the site structure or would occur also on a surface where the same stoichiometry would have been created thermally.

3.2.3. H_2/D_2 scrambling

The case of H_2/D_2 scrambling (Fig. 7b, Table 3) is somewhat more complicated because with LT-MoS_2 the reaction data obtained under the conditions of the present study were affected by mass-transport limitations [14]. In a series extending over a wider temperature range (300–480 K) the Arrhenius plot was found to be curved, with an activation energy of 63 $kJ\,mol^{-1}$ found below 373 K instead of 17 $kJ\,mol^{-1}$ around 470 K [14]. Over m-MoS_2, H_2/D_2 scrambling was much slower than over LT-MoS_2, and the temperature dependence of the rate constant was larger. The 75 $kJ\,mol^{-1}$ found after the $\mathbf{R}_{573}$ activation are quite near to the value obtained with LT-MoS_2 at lower temperatures. However, opposed to the observations with LT-MoS_2, the effect of $\mathbf{V}_{723}/\mathbf{R}_{573}$ on the scrambling activity was different from that of $\mathbf{R}_{573}$, the resulting activity was smaller and the activation energy even larger, which can be safely stated despite the low number of data points available (the activation energy would exceed 75 $kJ\,mol^{-1}$ even if any one of the three points was omitted). This suggests that the data measured with m-MoS_2 after $\mathbf{R}_{573}$ are still subject to mass-transfer influences; indeed, the corresponding Arrhenius plot shows a slight curvature, which is, however, hardly significant at the present level of experimental accuracy. Thus, despite the large uncertainties in the activation energy estimated for the $\mathbf{V}_{723}/\mathbf{R}_{573}$ activation (130 $kJ\,mol^{-1}$), one may conclude that the intrinsic activation energy of H_2/D_2 scrambling over MoS_2 is even larger than 75 $kJ\,mol^{-1}$.

Whereas the actual reaction kinetics of H_2/D_2 scrambling over both types of MoS_2 will require additional study, the data given in Fig. 7b and Table 3 are sufficient in the present context where only qualitative rankings of activation effects will be discussed. This ranking is clearly different between LT-MoS_2 and m-MoS_2: both activations had approximately the same effect on the former (which was confirmed in experiments with different degree of mass-transport influence [14]) whereas the milder treatment ($\mathbf{R}_{573}$) was much more effective with the latter. According to [14], H_2/D_2 scrambling may occur both on ^{2}M and ^{3}M sites; on this basis, the fact that the more severe activation ($\mathbf{V}_{723}/\mathbf{R}_{573}$) resulted in lower activity may be explained by an assumption mentioned above: the formation of inactive (or less active) sites of excessive Mo exposure (^{4}M). On LT-MoS_2, the majority of Mo_{cus} appears to be ^{2}M or ^{3}M irrespective of the activation procedure used, and the different ratio between both sites after the activations explains the differences in hydrogenation activity at comparable H_2/D_2 scrambling rates. On the sulfur-deficient surface of m-MoS_2, a loss of active sites appears to come into play. Apparently, $\mathbf{V}_{723}/\mathbf{R}_{573}$ converts ^{2}M into ^{3}M, and ^{3}M into ^{4}M sites, which would explain a loss of scrambling activity and a smaller hydrogenation activity than achievable with LT-MoS_2 at optimum activation (*vide supra*).

3.2.4. Isomerization of 2-methyl-1-butene

The isomerization of 2-methyl-1-butene has been suggested by Tanaka et al. [16] to be catalyzed by Brønsted sites of MoS_2. This assignment was supported by the observations that this reaction is neither accelerated by gas-phase hydrogen nor poisoned by oxygen and proceeds on the as-prepared catalyst without any thermal activation unlike the reactions discussed so far. We have confirmed these observations in our own work with different batches of LT-MoS_2 [15].

Beyond these qualitative experiments, a reliable characterization of MoS_2 with respect to its activity in 2-methyl-1-butene isomerization appears to be difficult. There was significant deactivation which clearly affects batch experiments at 373 K (see runs with LT-MoS_2* in Fig. 8a). At lower temperatures, the gas-chromatographic analysis showed that up to 40% of the hydrocarbon dosed into the cycle had been adsorbed on the catalyst surface at the time of the first analysis (2 min) [15]. As this adsorption was stronger when the catalysts had undergone thermal activations, one may conclude that the adsorption occurred mainly on Mo_{cus} sites. However, 2-methyl-1-butene isomerization which requires acidic sites was also deactivated. With the standard LT-MoS_2, we attempted to stabilize the activity by exposing the catalyst to the reaction mixture overnight. After this treatment, the catalyst ex-

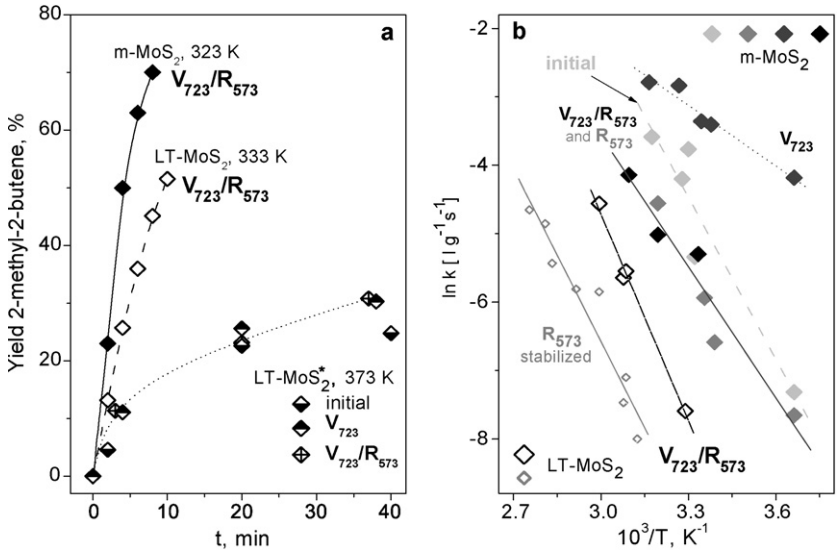

Fig. 8. Relation between activation procedure and catalytic activity for ball-milled MoS_2 (m-MoS_2) and LT-MoS_2, made by low-temperature decomposition of ATM: (a) isothermal runs (batch recycle reactor) MoS_2 of different activation and preparation, (b) temperature dependence of reaction rate measured over m-MoS_2 and LT-MoS_2 after different activations. For details about experimental problems and accuracy of data cf. text.

hibited appreciable residual activity, but deactivation could still be observed. The data presented below were therefore measured with non-stabilized catalysts (1st or 2nd run) except if specified otherwise (LT-MoS_2, after $\mathbf{R}_{573}$, cf. Fig. 8b).

Fig. 8a shows the development of the 2-methyl-2-butene yield with reaction time measured over different MoS_2 batches. The two LT-MoS_2 batches employed were very different, the reaction temperatures required to achieve comparable initial reaction rates differed by 40 K. For LT-MoS_2*, runs with different activation treatments are included, and it can be seen that the treatment had no significant influence on the activity although there may be a difference in the deactivation rate (see points at 40 min). A third batch prepared by the same route (labeled $MoS_2(A_2)$ in [14], data not included in Fig. 8a) yielded a third activity level between those shown in Fig. 6a [15]. Hence, 2-methyl-1-butene isomerization proceeded over LT-MoS_2 at rates varying strongly among different batches. Over m-MoS_2, the reaction was more rapid than over any of the LT-MoS_2 batches studied.

In Fig. 8b, the temperature dependence of 2-methyl-1-butene isomerization is presented for m-MoS_2 and LT-MoS_2. Due to the above mentioned experimental problems, the rate constants plotted should be considered as estimates rather than as accurate kinetic data. With m-MoS_2, reductive activation caused a slight loss of activity compared with the initial state. Surprisingly, mere thermoevacuation ($\mathbf{V}_{723}$) led to a real boost in activity, which was quenched when the surface was subsequently reduced ($\mathbf{V}_{723}/\mathbf{R}_{573}$). The difference between the different activations of LT-MoS_2 may arise from the overnight stabilization applied in the series with $\mathbf{R}_{573}$ activation (*vide supra*). The data have been included only to demonstrate the order of magnitude of the activation energy. All Arrhenius plots except that of m-MoS_2 after $\mathbf{V}_{723}$ have approximately the same gradient. Therefore, given the large experimental uncertainties in the kinetic experiments with 2-methyl-1-butene isomerization (*vide supra*), it can be concluded that the activation energy of this reaction does not depend on the pretreatment and is in the order of 50–60 kJ mol^{-1}. The measurements with m-MoS_2 after $\mathbf{V}_{723}$ were apparently affected by mass-transfer limitations.

These results cannot be easily reconciled with the notion of structural Brønsted sites being active centers for the 2-methyl-1-butene isomerization. According to theoretical studies [26,27], the only type of hydrogen-containing species on the MoS_2 surface are edge-plane SH groups, basal-plane SH groups being unstable. The existence of Mo–H, which would not be a Brønsted site anyway is questionable in a hydrogen-free atmosphere and at low degrees of coordinative unsaturation. Therefore, if acidic –SH groups are to be identified as active sites, some relation between the amount of exchangeable hydrogen on the MoS_2 surface and the isomerization activity should exist, but it could not be observed. It has been shown in [18] that $\mathbf{V}_{723}$ resulted in very low amounts of exchangeable hydrogen on LT-MoS_2, which is plausible for a material that had not been in contact with hydrogen before and should therefore hold also for m-MoS_2. Here, however, the highest reaction rates were observed just after $\mathbf{V}_{723}$. Moreover, after reductive activation, the concentration of exchangeable hydrogen was smaller on m-MoS_2 than on LT-MoS_2 (Table 2), but the former was more active.

On the other hand, there was no correlation between 2-methyl-1-butene isomerization activity and the concentration of Mo_{cus} either. The reaction proceeded on the initial surfaces which have no oxygen chemisorption capacity at all, and it was not poisoned by oxygen. Therefore, catalysis by Mo-organic intermediates or by Lewis sites can be ruled out as well. The acidity reflected in the test reaction was apparently a Brønsted acidity, and we believe that it is related to a type of site not present on regular surfaces, i.e., it arises from structural defects. The poor reproducibility of the isomerization rate and the particular activity obtained by the mechanochemical treatment support this view.

Any more detailed description of the site will, however, remain speculative on the basis of the present data. Bending of nanoslabs, which may affect acidity as well, was present both in m-MoS_2 and in LT-MoS_2 and can, therefore, not explain the differences observed. Impact-related defect structures in MoS_2 which create more rim Mo sites (Fig. 4b) seem to offer a better approach to explain differing results. A candidate for the active site might be Mo-OH defect groups because on all surfaces studied by XPS, O 1s signals with very low intensity could be detected, which were too weak and unspecific for quantitative studies [15]. The higher activity of the initial m-MoS_2 as compared to the reduced state (Fig. 8b) may have originated from the presence of sulfate species (*vide supra*). The particular success of $\mathbf{V}_{723}$ in the activation of m-MoS_2 for 2-methyl-1-butene isomerization is not easily explained. A possible hint may come from former studies where Mo in higher oxidation states (Mo(VI)) was found after thermo-

evacuation of sulfate-containing MoS_2 surfaces [18,28]. The higher oxidation state might increase the strength of the acid defect sites.

3.3. Outlook

The data presented above demonstrate that the impact of mechanical energy transformed a catalytically completely active microcrystalline MoS_2 into an active hydrogenation catalyst, which was to be expected on the background of the literature [12,13]. More remarkable are the strongly different effects of the mechanochemical treatment on other test reactions: H_2/D_2 scrambling was activated to a much smaller extent, and while the hydrogenation activity competed with the best performance obtained with a reference catalyst (LT-MoS_2), the scrambling activity remained far below the standard. *cis–trans* isomerization of *cis*-but-2-ene, which was definitely catalyzed by LT-MoS_2, did not occur at all over m-MoS_2. This confirms our earlier conclusion that these reactions use different sites (hydrogenation—^{3}M sites, H_2/D_2 scrambling—^{2}M and ^{3}M sites, *cis–trans* isomerization—^{1}M sites [14]) and may be employed to trace these sites on unknown MoS_2 surfaces. On this basis, the site structure of m-MoS_2 can be characterized more in detail: It was dominated by ^{3}M sites, with ^{2}M sites (and, possibly, also ^{4}M sites, see above) present as well, but without ^{1}M sites in significant quantities.

Although it is not possible so far to determine absolute amounts of these sites due to missing calibration of the reaction rates with surfaces of known site structure, the comparison of reaction rates (related to OCS capacities) is a useful new tool for the characterization of site structures on the surfaces of MoS_2 and, possibly, on other sulfide catalysts as well. The present study has left several relevant questions to be answered. First, due to the blockage of coordinatively unsaturated sites, probably by oxygen, we had to use thermal activations to clean the surface and find catalytic activity. These procedures might already have changed the initial site structure. While we employed standard procedures in this first attempt, further work would have to deal with possible impacts of this step and to device more conservative activations. Further, a comparison between an equilibrium and a non-equilibrium site structure would require the S/Mo ratios of both surfaces to be comparable. For our LT-MoS_2, however, data were available only for S/Mo ≈ 2. From the TEM results presented above, a direct comparison of m-MoS_2 and LT-MoS_2 would be appealing: while the size and curvature of the nanoslabs appears to be similar, the abundance of defects apparently originating from mechanical impact (cf. Fig. 4b) may differ and cause different activities just for reactions that require large sites (e.g., hydrogenation). Earlier studies with LT-MoS_2 gave evidence about coalescence and disappearance of surface defects on LT-MoS_2 [14,18]. Future studies, which are now under way, may show if and under which conditions such defect migration will lead to an equalization of differences in equilibrium and non-equilibrium site structures.

4. Conclusions

Microcrystalline MoS_2 obtained by high-temperature decomposition of $(NH_4)_2MoS_4$ (ATM), which was completely inactive in hydrocarbon transformations and H_2/D_2 scrambling after standard reductive activation treatments, has been transformed into an active catalyst by high-energy ball milling. The treatment, which caused the creation of bent MoS_2 nanoslabs with a multitude of defects, resulted in a considerable sulfur deficit (S/Mo = 1.8), an increase of the external surface area and the development of oxygen chemisorption capacity and hydrogen uptake after standard reductive activations. The activity pattern observed showed a very different effect of the mechanochemical treatment on the test reactions used, and it deviated strongly from that known from a reference MoS_2 made by low-temperature decomposition of ATM. After identical reductive activations, the mechanochemically treated MoS_2 was more active than the latter in ethylene hydrogenation and in 2-methyl-1-butene isomerization. It was less active in H_2/D_2 scrambling and had no activity at all for the *cis–trans* isomerization of 2-butene, which was clearly observed with the reference catalyst. This activity pattern implies that the mechanochemical treatment of microcrystalline MoS_2 left the Mo sites exposed with a larger degree of coordinative unsaturation than on the surface of the reference material; in particular, sites with only one sulfur vacancy were absent. The plausibility of this conclusion supports the eligibility of the use of some of these reactions (ethylene hydrogenation, H_2D_2 scrambling, *cis–trans* isomerization of 2-butene) to detect sites with different degree of coordinative unsaturation. Opposed to this, the isomerization of 2-methyl-1-butene seems to be inappropriate for the detection of acidic sites inherent to the MoS_2 surface. Instead, our results suggest that it is catalyzed by acidic sites related to structural defects.

Acknowledgments

Financial support by the German Science foundation is gratefully acknowledged (grants No. Gr 1447/15 and Be-1653/11). We would like to thank Ms. Susanne Buse for the physisorption measurements, Mrs. V. Duppel for practical TEM work and Prof. Dr. Dr. h.c. mult. A. Simon for enabling the TEM examinations.

References

[1] Y.G. Shirokov, Russ. J. Appl. Chem. 70 (1997) 919.
[2] Q.W. Zhang, F. Saito, J. Alloys Compd. 297 (2000) 99.
[3] A. Trovarelli, F. Zamar, J. Llorca, C. de Leitenburg, G. Dolcetti, J.T. Kiss, J. Catal. 169 (1997) 490.
[4] T. Ichikawa, N. Hanada, S. Isobe, H.Y. Leng, T. Ichikawa, Mater. Trans. 46 (2005) 1.
[5] J.J.A. Dusseault, C.C. Hsu, J. Macromol. Sci.-Rev. Macromol. Chem. Phys. C 33 (1993) 103.
[6] J. Haber, V.A. Zazhigailov, J. Stoch, L.V. Bogutskaya, I.V. Batcherikova, Catal. Today 33 (1997) 39.
[7] S. Soiron, L. Aymard, A. Rougier, J.M. Tarascon, Top. Catal. 16 (2001) 391.
[8] O.V. Krylov, A.A. Firsova, A.A. Bobyshev, V.A. Radtsig, D.P. Shashkin, L.Y. Margolis, Catal. Today 13 (1992) 381.
[9] S. Indris, R. Amade, P. Heitjans, M. Finger, A. Haeger, D. Hesse, W. Grünert, A. Börger, K.D. Becker, J. Phys. Chem. B 109 (2005) 23274.
[10] C.J.H. Jacobsen, J.Z. Jiang, S. Morup, B.S. Clausen, H. Topsoe, Catal. Lett. 61 (1999) 115.
[11] H.L. Castricum, H. Bakker, B. van der Linden, E.K. Poels, J. Phys. Chem. B 105 (2001) 7928.
[12] Y. Kuriki, K. Uchida, E. Sekreta, S. Ohshima, M. Yumura, F. Ikazaki, Fuel Process. Technol. 59 (1999) 189.
[13] M. Kouzu, K. Uchida, Y. Kuriki, F. Ikazaki, Appl. Catal. A 276 (2004) 241.
[14] M. Polyakov, M. Poisot, W. Bensch, M. Muhler, W. Grünert, J. Catal. 256 (2008) 137.
[15] M. Polyakov, Ph.D. thesis, Ruhr University, Bochum (2007).
[16] K.-I. Tanaka, T. Okuhara, Catal. Rev.-Sci. Eng. 15 (1977) 249.
[17] D.G. Kalthod, S.W. Weller, J. Catal. 95 (1985) 455.
[18] M. Polyakov, M.W.E. van den Berg, T. Hanft, M. Poisot, W. Bensch, M. Muhler, W. Grünert, J. Catal. 256 (2008) 126.
[19] J. Gjonnes, V. Hansen, A. Krerneland, Microsc. Microanal. 10 (2004) 16.
[20] R. Vincent, P.A. Midgley, Ultramicroscopy 53 (1994) 271.
[21] C. Own, Ph.D. thesis, Northwestern University, Evanston, IL, 2005.
[22] E.P. Barrett, L.G. Joyner, P.P. Halenda, J. Am. Chem. Soc. 73 (1951) 373.
[23] R.L. Wilson, C. Kemball, A.K. Galwey, Trans. Faraday Soc. 58 (1962) 583.
[24] B. Schönfeld, J.J. Huang, S.C. Moss, Acta Crystallogr. B 39 (1983) 404.
[25] L. Jalowiecki, A. Aboulaz, S. Kasztelan, J. Grimblot, J.P. Bonelle, J. Catal. 120 (1989) 108.
[26] L.S. Byskov, J.K. Norskov, B.S. Clausen, H. Topsoe, J. Catal. 187 (1999) 109.
[27] L.S. Byskov, M. Bollinger, J.K. Norskov, B.S. Clausen, H. Topsoe, J. Mol. Catal. A 163 (2000) 117.
[28] F. Maugé, J. Lamotte, N.S. Nestorenko, O. Manoilova, A.A. Tsyganenko, Catal. Today 70 (2001) 271.